JOURNAL OF PROPULSION AND POWER
Vol. 21, No. 2, March–April 2005 (Tentative)

Nonthermal Ignition of Premixed Hydrocarbon–Air Flows by Nonequilibrium Radio Frequency Plasma

Naveen Chintala,* Rod Meyer,† Adam Hicks,‡ Ainan Bao,§ J. William Rich,¶ Walter R. Lempert,** and Igor V. Adamovich††
The Ohio State University, Columbus, Ohio 43210-1107

Results are presented of nonequilibrium rf plasma assisted combustion experiments in premixed air–fuel flows. The experiments have been conducted in methane–air, ethylene–air, and CO–air mixtures. The results show that large volume ignition by the uniform and diffuse rf plasma can be achieved at significantly higher flow velocities (up to $u = 25$ m/s) and lower pressures ($P = 60$–130 torr) compared to both a spark discharge and a dc arc discharge. The experiments also demonstrated flame stabilization by the rf plasma, without the use of any physical obstacle flameholders. Fourier transform infrared (FTIR) absorption spectra of combustion products show that a significant fraction of the fuel (up to 80%) burns in the test section. Temperature measurements in the diffuse rf discharge using FTIR emission spectra show that the flow temperature in the plasma before ignition ($T = 250$–$550°$C at $P = 60$–120 torr) is considerably lower than the autoignition temperatures for ethylene–air mixtures at these pressures ($T = 600$–$700°$C). Visible emission spectroscopy measurements in C_2H_4–air flows in the rf discharge detected presence of radical species such as CH, C_2, and OH, as well as O atoms. In CO–air flows, O and H atoms have been detected in the rf plasma region and CO_2 emission (carbon monoxide flame bands) in the flame downstream of the rf plasma.

I. Introduction

CONTROL of ignition and combustion processes in aircraft jet engines is of crucial importance for their performance over a wide range of operation parameters, such as altitude, flight speed, and thrust. Reduction of ignition delay time, flameholding and flame stability improvement, flame blowoff prevention, possibility of high-altitude relight, and extension of fuel flammability limits are some of the key technical issues in this field.

The most common approaches to ignition of combustible mixtures are 1) the use of heated surfaces or filaments, 2) pilot flames, 3) spark discharges and plasma torches, and 4) laser-induced spark. A problem common for all of these methods, which are based on purely thermal ignition mechanisms, is that ignition occurs only in a small volume of the flow, which may result in an incomplete combustion due to the slow lateral flame propagation speed compared to the axial flow velocity.

Chemically active radicals in a combustible mixture can be also produced by nonthermal methods, such as laser photodissociation or electron impact dissociation in an electric discharge. Several studies of photochemical ignition of H_2–O_2, H_2–air, and CH_4–O_2 mixtures (with and without additives such as O_3 and NH_3) using excimer lasers[1–4] suggested that photochemical ignition can be achieved at lower laser pulse energies than would be required for thermal ignition.[3] At these conditions, the primary radicals produced by photodissociation are O and H atoms. Photochemical ignition of these mixtures occurs only when high radical concentrations (of the order of 10^{17} cm^{-3}) (Refs. 1–4) are produced. Both minimum laser pulse energy and minimum radical concentrations are sharply reduced if the combustible mixture is independently preheated up to several hundred degrees centigrade (Ref. 4). Qualitatively, this may occur because at low temperatures the radical recombination rates are faster than the rates of chemical reactions between the radicals and stable molecules. Preheating allows a larger fraction of the primary radicals formed by photodissociation to participate in the latter reactions.

The use of onboard excimer lasers for ignition in jet engines appears impractical. On the other hand, using nonequilibrium plasmas for initial radical production in combustible mixtures can be attractive for practical applications, especially if such plasmas can be sustained in large volumes and at reasonable power budget. Reaching comparable levels of radical concentrations ($\sim 10^{17}$ cm^{-3}) using nonequilibrium electric discharges requires operation at both high values of the reduced electric fields, $E/N \sim 10^{-15}$ V·cm^2, when electron impact dissociation efficiency peaks[5,6] and at high specific energy loading in the discharge, $\sim$0.1–0.2 J/cm^3 at $P \sim 1$ atm. However, high-energy loading typically causes constriction of high-pressure discharges with the rapid ionization instability development. Constriction limits the discharge volume and generates intense localized joule heating, resulting in "regular" thermal ignition confined to a small volume, similar to the spark ignition.

In our recent work[7–11] (also see Ref. 12), operation of a uniform stable nonequilibrium rf discharge generated in cold steady-state supersonic airflows and operated at high *E/N* was demonstrated. The stability of this transverse rf discharge is greatly enhanced by two factors, 1) the use of dielectric covered plane electrodes flush mounted in the test section walls and 2) aerodynamic stabilization, that is, dissipation of incipient arc filaments by the fast gas flow perpendicular to the direction of electrical current. In particular, stable and uniform transverse rf plasmas have been generated in steady-state cold supersonic flows of methane and air at $M = 1.5$–4.0, at test section pressures of up to $P = 0.1$–0.2 atm, temperatures of $T = 100$–200 K, plasma volumes of 5–10 cm^3, and electron densities of up to $n_e = 3 \cdot 10^{11}$ cm^{-3} (Ref. 9). The estimated reduced electric field in this discharge is $E/N \sim 10^{-15}$ V·cm^2, whereas the gas temperature rise in the discharge did not exceed $\Delta T \sim 50$ K. These high values of *E/N* imply that a substantial fraction of the input discharge power goes to electronic excitation and molecular

Presented as Paper 2004-0835 at the AIAA 42nd Aerospace Sciences Meeting and Exhibit, Reno, NV, 5–8 January 2004; received 13 May 2004; revision received 16 September 2004; accepted for publication 14 December 2004.

Copies of this paper may be made for personal or internal use, on condition that the copier pay the $10.00 per-copy fee to the Copyright Clearance Center, Inc., 222 Rosewood Drive, Danvers, MA 01923; include the code 0748-4658/05 $10.00 in correspondence with the CCC.

Q1 *(**Job title**), Department of Mechanical Engineering, Nonequilibrium Thermodynamics Laboratories.
Q2 †(**Job title**), Department of Mechanical Engineering, Nonequilibrium Thermodynamics Laboratories.
Q3 ‡(**Job title**), Department of Mechanical Engineering, Nonequilibrium Thermodynamics Laboratories.
Q4 §(**Job title**), Department of Mechanical Engineering, Nonequilibrium Thermodynamics Laboratories.
Q5 ¶(**Job title**), Department of Mechanical Engineering, Nonequilibrium Thermodynamics Laboratories.
Q6 **(**Job title**), Department of Mechanical Engineering, Nonequilibrium Thermodynamics Laboratories.
Q7 ††(**Job title**), Department of Mechanical Engineering, Nonequilibrium Thermodynamics Laboratories.

dissociation by electron impact[5,6] with subsequent generation of chemically active radical species. This may well affect the ignition chemistry and, therefore, the ignition delay time. Indeed, kinetic modeling of a pulsed discharge ignition of a stoichiometric CH_4–air mixture[11,12] suggests the importance of molecular dissociation in the plasma for ignition kinetics. In these calculations, a constant-volume stoichiometric methane–air mixture, initially at $P = 0.1$ atm, $T = 300$ K, was excited by a pulsed discharge. The discharge *E/N* was modeled by a Gaussian shape pulse, with the full with at half-maximum of 7 μs and peak value of $E/N = 10^{-15}$ V · cm^2. The kinetic mechanism used in these calculations was GRI-Mech 3.0,[13] with additional N_2, O_2, and CH_4 electron impact excitation, dissociation, and ionization reactions incorporated. The rate coefficients of these reactions have been evaluated using experimental electron impact cross sections averaged over the electron energy distribution function (EEDF) obtained from the solution of the Boltzmann equation for the plasma electrons for given *E/N* (Refs. 5 and 6). Because in these calculations the effect of electronically excited nitrogen molecules on oxygen dissociation was not taken into account, they represent a lower bound of the effect of O and H atoms on the methane ignition kinetics. From Fig. 1, it can be seen that that the voltage pulse generates radical concentrations (O and H atoms and OH) of up to $\sim 10^{16}$ cm^{-3}. In addition, these calculations suggest that inhibiting electron impact dissociation reactions of methane and oxygen while keeping joule heat generated by the pulse constant considerably increases ignition delay time, from 2.5 to about 100 ms (Fig. 2). In Fig. 2, the initial gas temperature rise is due to joule heating by the pulse discharge, whereas the second rise is due to ignition of the mixture. This demonstrates the importance of key radical generation for the plasma ignition processes.

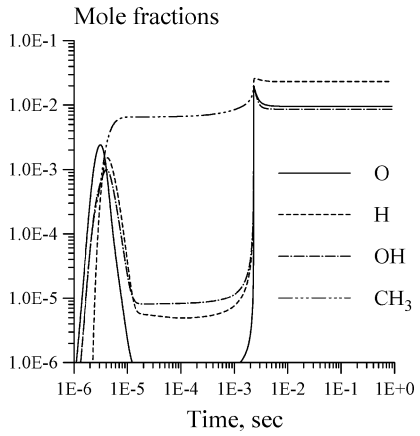

Fig. 1 Radical species mole fractions generated in pulsed discharge in stoichiometric CH_4–air mixture, $P = 0.1$ atm, $E/N = 10^{-15}$ V · cm^2, pulse duration $\tau = 7$ μs.

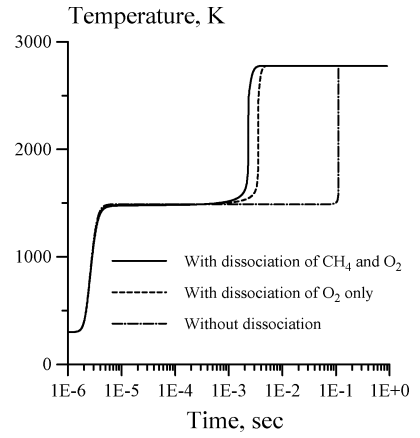

Fig. 2 Effect of inhibiting electron impact dissociation of methane and oxygen on gas temperature and ignition delay time; Fig. 1 conditions.

The main objectives of the present work are 1) to determine experimental conditions, such as pressures, flow velocities, and discharge powers, when nonequilibrium rf discharge plasmas can produce ignition in premixed hydrocarbon–air flows; 2) to measure the flow temperature in the rf discharge, which would determine whether the ignition mechanism is thermal or not; and 3) to detect presence of chemically active radicals and atoms that may participate in the nonthermal ignition process.

II. Experimental

The experiments are conducted at a new high-speed flow plasma combustion facility recently developed at The Ohio State University (OSU).[14,15] A schematic of the OSU high-speed flow steady-state plasma combustion facility is shown in Fig. 3. A premixed hydrocarbon–air flow enters the 5 × 1 cm rectangular cross section, 20-cm-long test section through a 50 ft long, 1-in.-diam corrugated gas supply line. A spring-loaded shutoff valve and a flash arrester installed in the $\frac{1}{4}$-in.-diam hydrocarbon gas supply line enable quick flow shutoff and prevent the flame propagation into the hydrocarbon gas cylinder. Downstream of the test section, the flow is diluted with atmospheric air through the vent valve to prevent further combustion in the vacuum system and in the dump tank (Fig. 3). The 1200-ft^3 dump tank is pumped out using an Allis–Chalmers 1300 cfm rotary vane vacuum pump. The test section static pressure ranges from 30 torr to 0.5 atm. The mass flow rate through the test section can be varied from below 1 g/s to 12 g/s. The test section pressure and the mass flow rate can be varied independently. This makes the experimental facility suitable for combustion studies both in high-speed, low-pressure and in low-speed, intermediate-pressure flows. At the highest mass flow rate and the lowest pressure, the experimental conditions correspond to the test section Mach number of $M \cong 0.9$. At the steady-state test section pressure of 100 torr, the mass flow rate through the vent valve is approximately 100 g/s. For the baseline flow conditions, at a pressure of $P = 100$ torr, mass flow rate through the test section of $\dot{m} = 10$ g/s, and stoichiometric methane–air flow mixture (9.5% CH_4 in air), the air dilution reduces the methane fraction in the flow into the dump tank to about 1%, which is well below the low flammability limit of 5% (Ref. 16).

The test section made of high-temperature machinable mica ceramic and steel is shown in greater detail in Fig. 4. The flow enters the rectangular cross section test section through a ceramic honeycomb flow straightener (300 holes/in.^{2}) and passes between two rf electrode blocks. Each of the two 5 × 3 cm electrode blocks, manufactured of mica ceramic and flush mounted in the test section walls, incorporates three copper strip electrodes 45 mm long and 5 mm wide. The sectioned design of the electrodes allows sustaining both transverse and axial rf discharges in the test section. The electrodes are rounded at the edges to prevent high electric field concentration and hot spot formation in the plasma near the edges. The use of dielectric (ceramic) layers between the electrodes and the flow precludes secondary ionization from the electrode surfaces, which greatly improves the stability of the transverse rf discharge

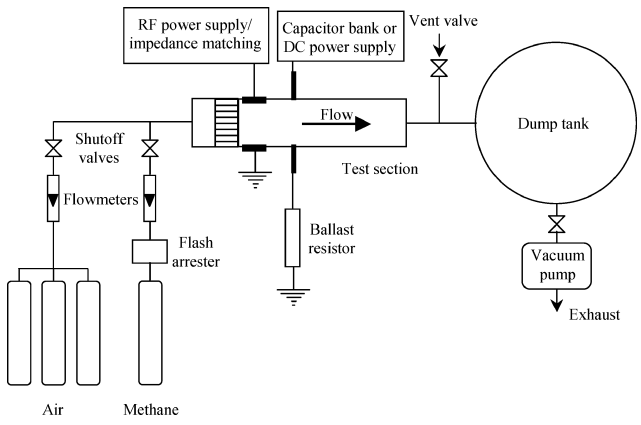

Fig. 3 Schematic of OSU high-speed plasma combustion facility.

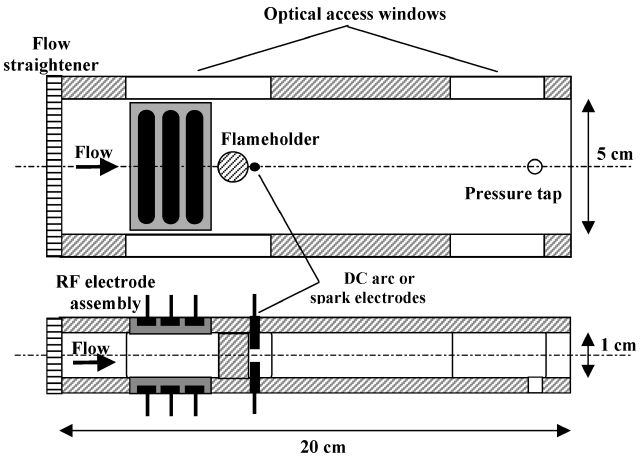

Fig. 4 Schematic of plasma assisted combustion test section.

sustained in the test section,[17] as well as allows scalability of the rf plasma volume. The rf electrodes shown in Fig. 4 are connected to a Dressler 5-kW, 13.56-MHz power supply through an automatic impedance matching network. In the present experiments, very good impedance matching has been achieved, with less than 1% of the input rf power reflected back. To prevent interference of the high-power rf discharge with the diagnostic equipment, the entire test section assembly can be shielded by a brass foil Faraday cage.

A $\frac{1}{2}$-in.-diam boron nitride cylindrical flameholder can be placed 5-mm downstream of the rf electrode, if necessary. Two 2-mm-diam threaded pin electrodes are located in the top and bottom test section walls downstream of the flameholder, as shown in Fig. 4. The pins can be moved in the tapped holes in the ceramic test section walls, so that the distance between them electrodes can be varied from about 1 to 10 mm. The flameholder and the pin electrodes have been placed in the test section to explore the possible effect of the rf plasma on the flame piloted using conventional ignition methods, a dc arc discharge, or a capacitor bank spark discharge between the pins. For dc arc ignition, the pin electrodes are placed 2 mm apart and connected to a DEL 2-kV, 3-A dc power supply operated in a current stabilized mode, through a 6-kΩ ballast resistor. For spark ignition, the pins are placed 5–10 mm apart and connected to a 2-μF capacitor bank through a 500-Ω ballast resistor. The capacitors are charged by a Kaiser Systems 30-kV, 2.5-kW power supply. The
Q13 spark is triggered by an EG&G TM-11A trigger module, which applies a breakdown voltage to the electrodes. In the presented experiments, the capacitor spark voltage was varied from 4.5 to 9.0 kV.

The entire upstream half of the test section (11 cm long), which incorporates the rf electrode blocks, the flameholder, and the spark electrodes, is made out of mica ceramic parts bolted together. The downstream half (9 cm long) is made of steel. The plasma combustion facility is designed for the use of spectroscopic flow diagnostics. In particular, the test section has four optical access window ports, two on each side, as shown in Fig. 4. This provides optical access to both the rf discharge/flame attachment region and the flow region ~10 cm downstream of the discharge. Visible emission spec-
Q14 troscopy measurements are made using a Roper Scientific optical multichannel analyzer with liquid nitrogen cooled charge-coupled device camera for a detector and a 0.5-m monochromator and plane
Q15 BK-7 glass optical access windows. Fourier transform (FT) infrared (IR) emission spectroscopy temperature measurements are made using Biorad 175C, a dynamic alignment FTIR spectrometer with liquid nitrogen cooled InSb detector and CaF_2 or MgF_2 optical access windows. A static pressure tap is placed at the downstream end of the test section. The pressure tap is also used to draw off a sample of the combustible mixture or of the combustion products into a 15-cm-long static absorption cell placed in the absorption compartment of the FTIR spectrometer. The sample temperature in the absorption cell is monitored by a thermocouple. FT absorption spectra have been used to monitor the combustion completeness. The entire test section is placed inside a transparent rectangular polycarbonate box as a safety measure.

Note that measurements of the gas temperature in the rf discharge are of key importance for the interpretation of the results of the present study. In particular, they would help isolating the effect of radical production on the ignition and flame characteristics, as opposed to a trivial effect of the flow preheating by the rf discharge.

III. Results and Discussion

A. Plasma Assisted Ignition

Experiments using conventional ignition methods, that is, dc arc and spark discharges, showed that in the present test section ignition and flameholding are achieved only at rather low flow velocities and relatively high pressures. In particular, in stoichiometric CH_4–air flows ignition is produced at $u \leq 4.3$ m/s, $P \geq 350$ torr, whereas in stoichiometric C_2H_4–air flows ignition is achieved at $u \leq 6.3$ m/s, $P \geq 240$ torr. At these conditions, which correspond to the mass flow rate through the test section of $\dot{m} = 1.2$ g/s, the flame was attached to a $\frac{1}{2}$-in.-diam flameholder. Increase of the mass flow rate above $\dot{m} = 1.2$ g/s resulted in the flame blowoff. Ignition by both of these methods was also produced in a CH_4–air flow at $u = 5.0$ m/s, $P = 300$ torr and in a C_2H_4–air flow at $u = 7.6$ m/s, $P = 200$ torr (same mass flow rate of $\dot{m} = 1.2$ g/s), but no flameholding was achieved. At high mass flow rates, $\dot{m} = 3$–10 g/s, initiation of a spark or the dc arc discharge in the flow did not result in ignition and flameholding in the test section, but instead produced explosion downstream of the test section, in the vacuum system, where the flow velocity is much lower.

No ignition has been achieved by any of these two methods at pressures below $P = 300$ torr in methane–air flow and below $P = 200$ torr in ethylene–air flow, at the same mass flow rate of $\dot{m} = 1.2$ g/s. In these experiments, the dc arc discharge current and power were up to 150 mA and 60 W, respectively, for the pin electrode gap of 2 mm. In the spark discharge experiments, the capacitor spark voltage was varied from 4.5 to 9.0 kV, and the pin electrode gap was varied from 5 to 10 mm. No effect of varying these parameters on ignition and flameholding has been detected. The low values of the flame blowoff velocity compared to the experimental correlation,[18] $u_{BO} \sim 100$ m/s for methane at $P = 0.1$ atm and flameholder diameter of 1 cm, are most likely due to the three-dimensional heat transfer from the recirculating flow behind the flameholder to the top and bottom test section walls, which are only 1 cm apart.

Nonequilibrium rf discharge ignition experiments have been conducted in stoichiometric methane–air, ethylene–air, and CO–air flows at the mass flow rates of $\dot{m} = 1.2$–2.0 g/s and pressures of $P = 45$–130 torr. With all three electrode pairs powered, the uniform transverse discharge spans nearly the entire flow through the test section (Fig. 5), for the flow velocities from 10 to 260 m/s ($M = 0.8$). The discharge produced ignition in stoichiometric ethylene–air mixtures at pressures ranging from $P = 60$ ($u = 24.6$) to $P = 130$ torr ($u = 11.7$ m/s). In stoichiometric methane–air and CO–air mixtures, rf ignition was produced at pressures of $P = 80$–130 torr and $P = 100$–130 torr, respectively. These results were obtained with the flameholder removed from the test section, which demonstrates that the rf plasma assisted ignition method does not require additional flameholding. Figures 6 and 7 show photographs of ethylene–air and CO–air flames initiated and stabilized by the transverse rf discharge. It can be seen that the flow is ignited at the upstream boundary of the plasma. The flame spans the cross section of the flow and occupies

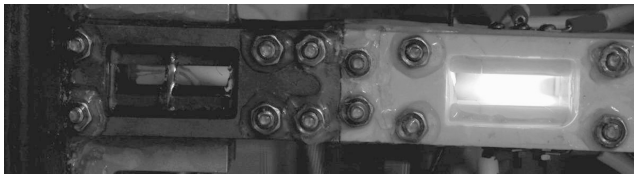

Fig. 5 Transverse rf discharge plasma (200 W) sustained in airflow, $P = 53$ torr, $u = 29$ m/s; plasma spans entire flow cross section (1 × 5 cm) with flow right to left.

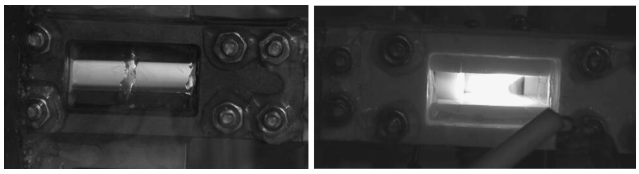

a) b)

Fig. 6 Stoichiometric air–ethylene mixture, $P = 120$ torr, $u = 12.7$ m/s, flow right to left: a) Transverse rf discharge plasma (200 W) and b) downstream flame region.

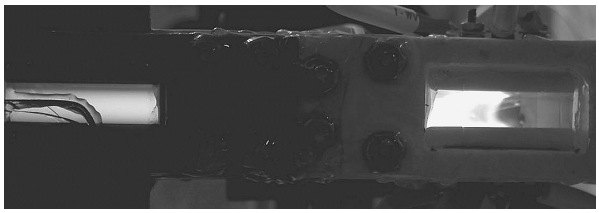

Fig. 7 Transverse rf discharge plasma (200 W) and flame in a stoichiometric air–CO mixture, $P = 117$ torr, $u = 12$ m/s; flow right to left.

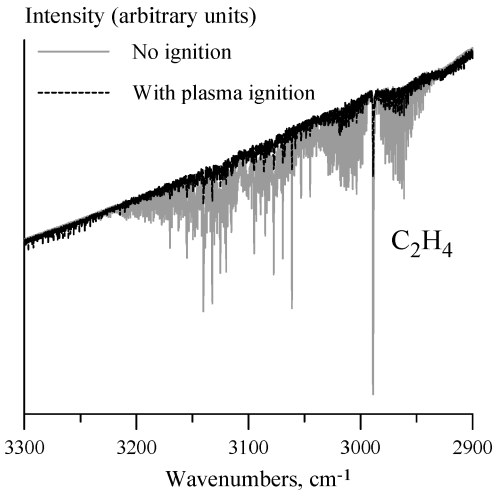

Q16 Fig. 8 Section of FTIR absorption spectra of Fig. 10 blown up, ethylene removal by plasma assisted combustion, $P = 70$ torr, mass flow rate 1.2 g/s, and rf power 200 W.

nearly the entire test section downstream of the discharge. Thus, the experiments demonstrate that the use of a diffuse rf discharge instead of a dc arc or a spark discharge allowed achieving large-volume ignition of stoichiomentric ethylene–air, methane–air, and CO–air flows at much higher flow velocities and lower pressures compared to the traditional ignition approaches (arc and spark discharges).

FTIR absorption spectra of plasma combustion products taken at these conditions provide additional evidence that plasma assisted ignition indeed occurs and show that a significant fraction of the fuel
Q17 burns in the test section. Figures 8 and 9 show FT absorption spectra of a stoichiometric ethylene–air mixture at P = 70 torr (without plasma ignition) and of the combustion products generated in the same mixture ignited by a 200-W rf discharge. At these conditions, the fraction of C_2H_4 burned in the test section is approximately 80% (Fig. 8), with significant amounts of combustion products such as CO, CO_2, and H_2O generated (Fig. 10). In stoichiometric methane–air mixtures, the burned CH_4 fractions are approximately 30% at $P = 90$ torr and 50% at $P = 100$ torr. Further quantitative analysis of the absorption spectra is underway.

We have also generated and sustained the rf plasma at higher test section pressures, up to $P = 220$ torr. However, above $P = 200$ torr the rf discharge impedance matching becomes increasingly difficult to control, which results in reduction of rf power coupled to the flow and extinguishing the plasma. Sustaining a stable and diffuse

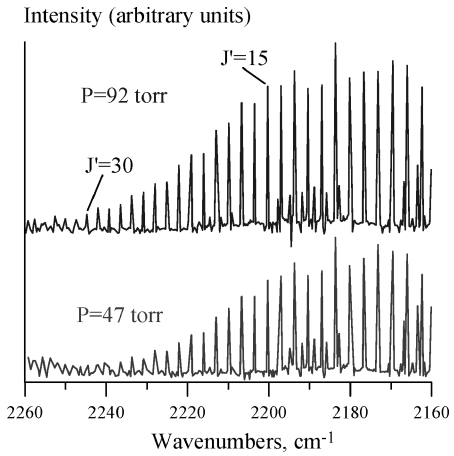

Fig. 9 Typical CO FTIR emission spectra at two different flow pressures, mass flow rate 1.2 g/s, RF power 200 W, and 1% CO in air. **Q18**

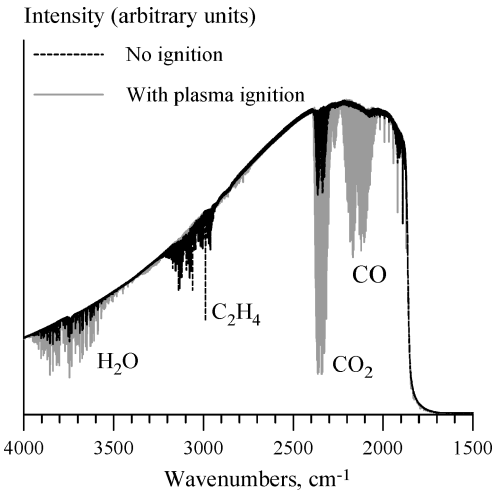

Fig. 10 FTIR absorption spectra of stoichiometric C_2H_4–air mixture (without ignition) and of plasma combustion products, $P = 70$ torr, mass flow rate 1.2 g/s, and rf power 200 W. **Q19**

self-sustained discharge in the high-pressure flows would require the use of a higher voltage, short pulse duration plasma generator.[17]

In the current experiments, the estimated minimum rf discharge energy loading per unit mass necessary for ignition is 200 W/1.2 g/s = 167 kJ/kg (or 0.05 eV/molecule). This is about 5.5% of the heat of combustion reaction for a stoichiometric ethylene–air mixture, 3025 kJ/kg.

B. FTIR Temperature Measurements

To determine the flow temperature in the RF discharge, we have used FT infrared spectroscopy. For this, carbon monoxide was added to the airflow as an infrared active thermometric species. The rotational temperature of the flow has been determined from the rotationally resolved R-branch of the CO fundamental band $1 \rightarrow 0$. At the relatively high static pressures in the test section ($P = 40$–130 torr), rotational relaxation time is much shorter than the flow residence time in the discharge (~10 ns vs ~1 ms), so that the single rotational–translational temperature is quickly established in the plasma. Previously, we have used this approach to measure temperature in the $M = 2$ nitrogen flows ionized by the transverse rf discharge.[8]

The main objective of these measurements was to determine the temperature in the rf discharge before fuel, that is, ethylene, methane, or CO, is added to the airflow. Obviously, adding the fuel species to the flow in the presence of the rf plasma may initiate exothermic plasmachemical reactions of these species with oxygen and radicals produced in the plasma (with or without ignition produced in the flow), thereby raising the flow temperature.

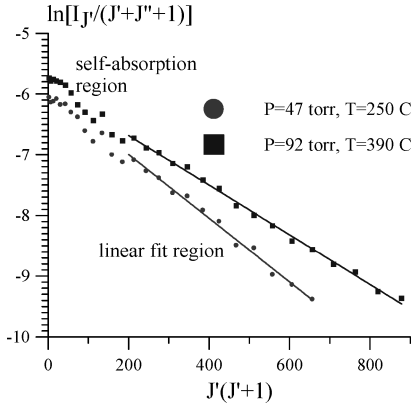

Fig. 11 Semilog Boltzmann plots for two spectra in Fig. 9.

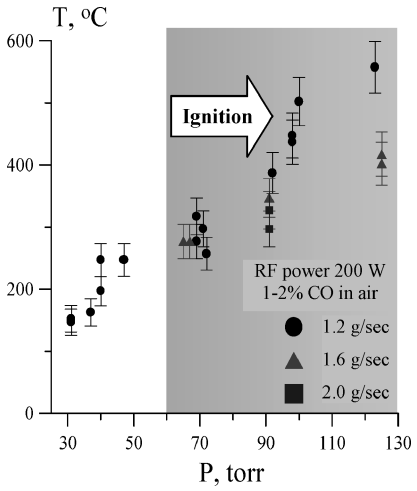

Fig. 12 Flow temperatures in transverse rf discharge in air at different pressures and mass flow rates, RF power 200 W, 1–2% CO in air.

Therefore, to minimize the temperature rise, as well as to reduce the self-absorption, for temperature measurements we have added small amounts of CO (1–2%) to the airflow.

Figure 9 shows typical CO FT infrared emission spectra at two different test section static pressures, $P = 47$ and $P = 92$ torr. At spectral resolution of 0.25 cm^{-1}, individual rotational peaks up to $J' = 30$–40, where J' is the upper rotational quantum number, are easily resolved and identified. To improve the signal-to-noise ratio, the IR signal has been collected over a time period of about 40 s, during which significant heating of the test section walls was detected. Therefore, the inferred temperatures are actually somewhat higher than the temperature in the rf discharge immediately after its initiation (and subsequent rapid ignition of the flow) in the initially cold test section. Figure 11 shows Boltzmann plots for these two spectra, that is, the dependence of the log of emission intensity from the upper rotational level J', $I_{J'}$, divided by the sum of the upper and the lower rotational quantum numbers, $J' + J'' + 1$, vs, $J'(J' + 1)$. The spectra appear as straight lines, with the slope proportional to the rotational temperature. The nonlinear behavior at the low J' value region of the spectra, which is not used for the temperature inference, is due to the self-absorption of the CO infrared radiation in the test section. The slope of linear region between $J' = 15$ and $J' = 30$–35 was used for the temperature inference. Because of the high signal-to-noise ratio and because as many as 15–20 rotational lines have been used for the temperature inference, the uncertainty of these measurements is rather small, ±5%.

Figure 12 shows the summary of the airflow temperature measurements at the static pressures of $P = 30$–125 torr and mass flow rates of $\dot{m} = 1.2$–2.0 g/s. Note that the inferred temperatures vary from $T = 150°C$ at $P = 30$ torr to $T = 400$–550°C at $P = 125$ torr. The shaded area in Fig. 12, that is, for $P > 60$ torr, shows the range of pressures when adding a stoichiometric amount of ethylene to the

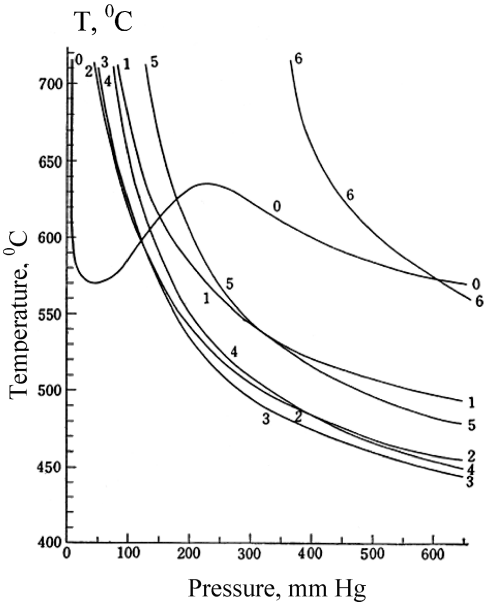

Fig. 13 Isochors for autoignition temperatures of ethylene–air mixtures 18: curve 0, 5% ethylene in air; 1, 10%; 2, 20%; 3, 30%; 4, 40%; 5, 50%; and 6, 60%.

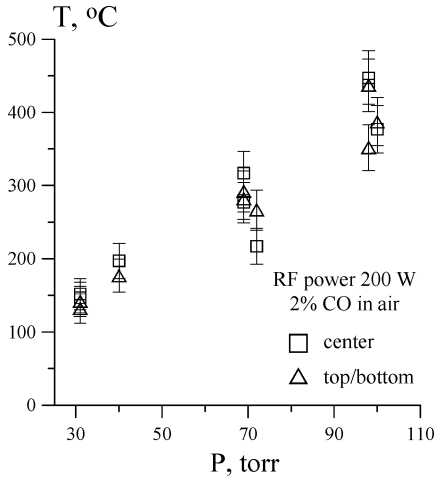

Fig. 14 Flow temperatures in transverse rf discharge in air measured in center of flow and in regions near rf electrodes, $\dot{m} = 1.2$ g/s, rf power 200 W, and 1–2% CO in air.

airflow in the rf discharge results in immediate flow ignition. This result is quite remarkable because the inferred flow temperatures (before the ignition) are much lower than the autoignition temperature of ethylene at these pressures (600–700°C, Fig. 13[19]). Note that at temperatures close to the autoignition temperature ignition delay time is typically of the order of a few seconds to a few tens of seconds,[19,20] whereas in the present experiments it is well below 1 s. The ignition delay time can be estimated from the residence time of the flow in the plasma, $\tau \sim L/u \sim 1$–3 ms, where $L \sim 3$ cm is the streamwise length of the plasma and $u \sim 10$–30 m/s is the flow velocity. These results strongly suggest that ignition in the hydrocarbon flows excited by nonequilibrium transverse rf discharge occurs by a nonthermal mechanism.

To estimate the transverse temperature nonuniformity in the rf discharge, we have measured the flow temperature in the plasma with the optical access window covered by one of two masks, one with a 5-mm-wide horizontal slit in the center, that is, midway between the top and bottom test section walls, and the other with two 2-mm-wide horizontal slits near the top and the bottom of the test section, that is, close to the rf electrode blocks (Fig. 4). The results are in Fig. 14, which shows the two temperatures to be very close (within 10%). This demonstrates that the nonuniform flow heating, that is,

hot spot formation, in the near-electrode regions of the rf discharge is insignificant and is, therefore, unlikely to affect flow ignition by the plasma. This result also suggests that ignition occurs in the entire volume of the plasma, not just near rf electrodes.

C. Visible Emission Spectroscopy Measurements

Visible emission spectra of the rf discharge plasmas have been obtained in air, ethylene–air, and CO–air mixtures at the mass flow rate of $\dot{m} = 1.2$ g/s, test section pressures between 40 and 120 torr (flow velocities from $u = 38$ m/s to $u = 12.7$ m/s), and rf discharge power of 200 W.

Figures 15–18 show a summary of the results obtained in ethylene–air flows. Note that CH (4300 A-band system), C_2 (Swan bands), and OH ($A^2\Sigma^+$-$X^2\Pi$ system) radicals are detected in the plasma. The C_2 Swan band system ($\Delta v = 0, \pm 1$), usually detected in hydrocarbon–air flames, is the most pronounced feature of the present ethylene–air rf plasma/flame spectra. Also, oxygen atoms have been detected in the air plasma. In Fig. 18, the O atom line at 777 nm can be clearly identified. At these conditions, O atoms in the plasma are most likely produced by direct electron impact dissociation of oxygen. Adding ethylene to the flow considerably reduces excited O atom emission (Fig. 18).

Figures 19–22 show the results obtained in CO–air flows. At these conditions, the CO angstrom band system, shown in Fig. 19, is the most prominent feature in the visible spectrum of the rf plasma/flame region (the upstream window in Fig. 7). Also, visible emission spectra of the rf discharge plasmas in air and CO–air mixtures indicate that both O and H atoms are generated in the plasma. Figure 20 shows a partially resolved triplet O atom line at 777 nm, which is detected both in air and in CO–air plasma flows. Similar to the ethylene–air mixtures, adding CO to the mixture reduces the O atom line intensity. Figure 21, which shows a comparison of visible emission spectra in

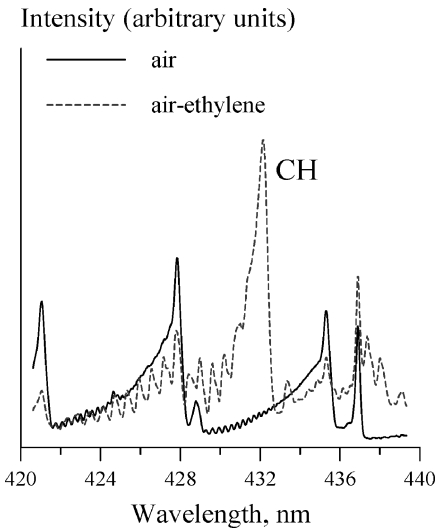

Q20 **Fig. 15 Emission spectra of rf discharge plasma in air and in stoichiometric ethylene–air mixture; CH bands, $P = 120$ torr, and rf power 200 W.**

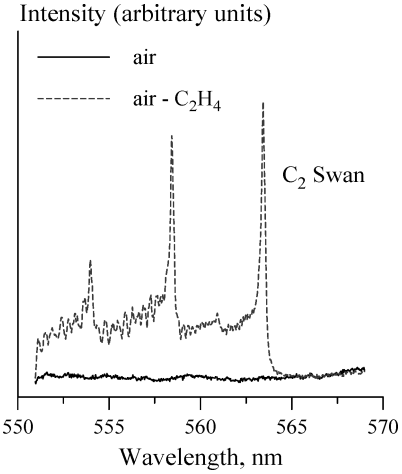

Q21 **Fig. 16 Emission spectra of rf discharge plasma in air and stoichiometric C_2H_4–air mixture; C_2 Swan bands, $P = 110$ torr, and rf power 200 W.**

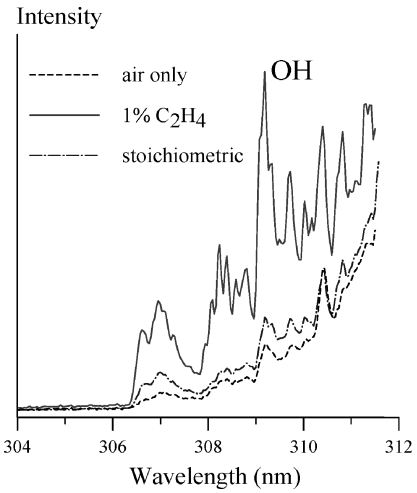

Fig. 17 Emission spectra of rf discharge plasma in air and etylene–air mixtures; OH bands, $P = 65$ torr, and rf power 200 W. **Q22**

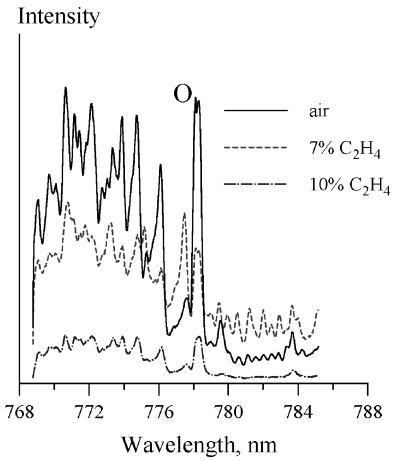

Fig. 18 Emission spectra of rf discharge plasma in air and C_2H_4–air mixtures, $P = 50$ torr, rf power 200 W. **Q23**

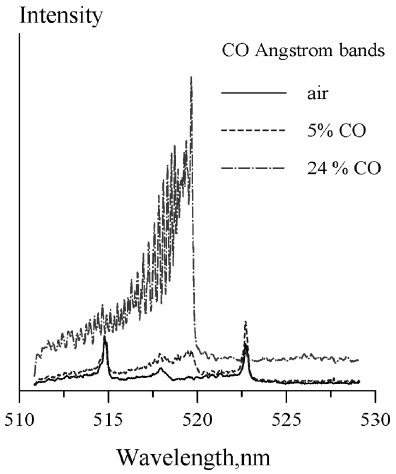

Fig. 19 Emission spectra of rf discharge plasma in air and CO–air mixtures, $P = 40$ torr, rf power 200 W. **Q24**

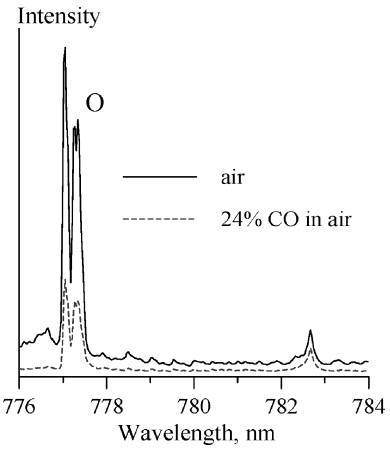

Q25 **Fig. 20 Emission spectra of rf discharge plasma in air and CO–air mixture (30% CO), $P = 40$ torr, rf power 200 W.**

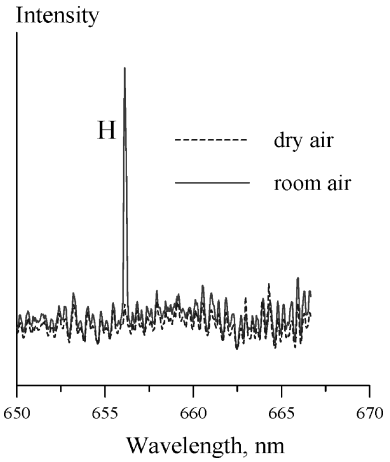

Q26 **Fig. 21 Emission spectra of rf discharge plasma in CO–room air mixture and CO–dry air mixture (20% CO), $P = 100$ torr, rf power 200 W.**

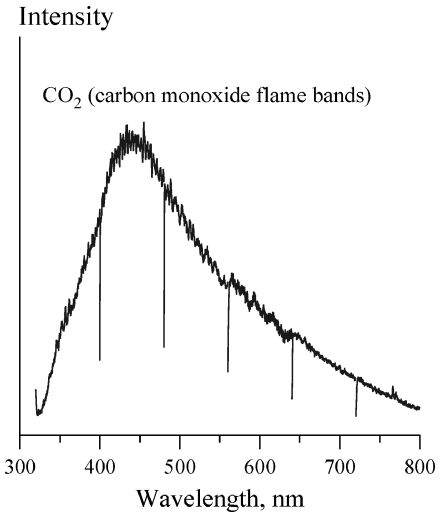

Fig. 22 Emission spectra of the flame in CO–air mixture (20% CO, far downstream of rf discharge), $P = 100$ torr, rf power 200 W.

CO/room air and CO/dry air mixtures, shows atomic hydrogen line at 566 nm in the rf plasma initiated in the presence of water vapor in the flow. Oxygen and hydrogen atoms in CO–air plasma flows are most likely produced by electron impact dissociation of O_2 and water vapor, respectively. Finally, CO–air visible emission spectra of the pale blue flame region downstream of the rf plasma region, taken through the downstream optical access window (Fig. 7), show well-pronounced CO_2 emission bands (carbon monoxide flame bands,[21]) typically detected in CO–air flames. At this resolution, these complex narrowband system appears as a broadband structure with a maximum at 420 nm. This provides additional evidence that CO–air mixtures are indeed ignited by the rf plasma and that the extended blue glow downstream of the plasma is indeed the flame and not the rf discharge afterglow.

These emission spectroscopy measurements serve only as a qualitative plasma diagnostic tool. Quantitative measurements of the radical and atom concentrations in the plasma require the use of highly sensitive absorption spectroscopy. These measurements would provide insight into kinetic mechanisms of ignition and combustion using low–temperature, nonequilibrium plasmas.

IV. Summary

The paper presents results of plasma assisted ignition and combustion experiments in premixed hydrocarbon–air and CO–air flows using both conventional ignition methods, such as a spark discharge and a dc arc discharge, and ignition by a nonequilibrium diffuse rf discharge spanning the flow. The experiments have been conducted in methane–air, ethylene–air, and CO–air flows at a new high-speed flow steady-state plasma combustion facility recently developed at OSU. The results show that large volume ignition of stoichiometric methane–air, ethylene–air, and CO–air flows by the uniform and diffuse rf plasma can be achieved at significantly higher flow velocities (up to $u = 25$ m/s) and lower pressures ($P = 60$–130 torr) compared to both spark discharge and dc arc discharge. The latter two approaches did not produce ignition at these conditions. FTIR absorption spectra of plasma combustion products show that a significant fraction of the fuel (up to 80%) burns in the test section.

During the rf plasma ignition, the flow is always ignited at the upstream boundary of the rf discharge and the flame occupied the entire test section downstream of the discharge. Thus, the experiments demonstrated flame stabilization by the rf plasma, without the use of any physical obstacle flameholders. Igniting of combustible mixtures right at the upstream boundary of the plasma also indicates that the ignition delay time is considerably shorter than that can be achieved with the traditional ignition methods. RF plasma ignition and combustion of these mixtures has been demonstrated both in room air and dry air.

Temperature measurements in the stable diffuse rf discharge using FTIR spectroscopy show that the flow temperature in the plasma before ignition ($T = 250$–550°C at $P = 60$–120 torr) is considerably lower than the autoignition temperatures for ethylene–air mixtures at these pressures ($T = 600$–700°C). Both the uncertainty and the run-to-run variation of these temperature measurements do not exceed a few percent. Spatially resolved temperature measurements obtained by masking the flow show the transverse temperature nonuniformity in the rf discharge to be insignificant.

Visible emission spectroscopy measurements in methane–air and ethylene–air flows in the rf discharge detected presence of radical species such as CH, C_2, and OH, as well as O atoms. In CO–air flows, O and H atoms have been detected in the rf plasma region and CO_2 emission (carbon monoxide flame bands) has been detected in the flame extending far downstream ($\sim$10–15 cm) of the rf plasma region.

The presence of O and H atoms, as well as OH radicals produced by electron impact dissociation in the rf plasma flows, together with the results of the temperature measurements discussed in Sec. III.B, suggest that these species may play a major role in nonthermal, large-volume ignition by the low-temperature rf plasma. Also, the results presented in Secs. III. A–III.C are consistent with the suggestions made in previous photochemical ignition measurements[4] and fast ionization wave ignition experiments,[22] that 1), preheating **Q27** the combustible mixture dramatically reduces the minimum radical concentrations necessary for ignition[4] and 2) adding active radicals species to the combustible mixture considerably reduces the ignition temperature and the ignition delay time.[22] Therefore, we **Q28** believe that combination of modest heating and active species generation by low-temperature nonequilibrium plasmas sustained in high-speed flows of combustible mixtures may be critical for the nonthermal, large-volume ignition.

Acknowledgments

This research has been supported by the Phase I Air Force Office of Scientific Research STTR Grant F49620-02-C-0054 and by the Dayton Area Graduate Studies Institute. We would like to express our sincere gratitude to Wonchul Lee and Yurii Utkin for numerous helpful suggestions.

References

[1]Lavid, M., and Stevens, J. G., "Photochemical Ignition and Premixed Hydrogen/Oxidizer Mixtures with Excimer Lasers," *Combustion and Flame*, Vol. 60, 1985, p.195.

[2]Lucas, D., Dunn-Rankin, D., Hom, K., and Brown, N. J., "Ignition by Excimer Laser Photolysis of Ozone," *Combustion and Flame*, Vol. 69, 1987, p. 171.

[3]Chou, M.-S., and Zukowski, T. J., "Ignition of $H_2/O_2/NH_3$, H_2/Air/NH_3, and $CH_4/O_2/NH_3$ Mixtures by Excimer-Laser Photolysis of NH_3," *Combustion and Flame*, Vol. 87, 1991, p. 191.

[4]Lavid, M., Nachson, Y., Gulati, S. K., and Stevens, J. G., "Photochemical Ignition of Premixed Hydrogen/Oxygen Mixtures with ArF Laser," *Combustion Science and Technology*, Vol. 96, 1994, p. 231.

[5]Aleksandrov, N. L., Vysikailo, F. I., Islamov, R. S., Kochetov, I. V., Napartovich, A. P., and Pevgov, V. G., "Discharge Model in a N_2:$O_2 = 4$:1 Mixture," *High Temperature*, Vol. 19, 1981, p. 485.

[6]Aleksandrov, N. L., Vysikailo, F. I., Islamov, R. S., Kochetov, I. V., Napartovich, A. P., and Pevgov, V. G., "Electron Distribution Function in a N_2:$O_2 = 4$:1 Mixture," *High Temperature*, Vol. 19, 1981, p. 22.

[7]Yano, R., Contini, V., Ploenjes, E., Palm, P., Merriman, S., Aithal, S., Adamovich, I., Lempert, W., Subramaniam, V., and Rich, J. W., "Supersonic Nonequilibrium Plasma Wind Tunnel Measurements of Shock Modification and Flow Visualization," *AIAA Journal*, Vol. 38, No. 10, 2000, pp. 1879–1888.

[8]Merriman, S., Ploenjes, E., Palm, P., and Adamovich, I. V., "Shock Wave Control by Nonequilibrium Plasmas in Cold Supersonic Gas Flows," *AIAA Journal*, Vol. 39, No. 8, 2001, pp. 1547–1552.

[9]Meyer, R., Palm, P., Ploenjes, E., Rich, J. W., and Adamovich, I. V., "The Effect of a Nonequilibrium RF Discharge Plasma on a Conical Shock Wave in a $M = 2.5$ Flow," *AIAA Journal*, Vol. 41, No. 5, 2003, pp. 465–469.

[10]Palm, P., Meyer, R., Ploenjes, E., Bezant, A., Adamovich, I. V., Rich, J. W., and Gogineni, S., "MHD Effect on a Supersonic Weakly Ionized Flow," Paper 2002-2246, 33rd Plasmadynamics and Lasers Conf., May 2002.

[11]Adamovich, I. V., Rich, J. W., and Nelson, G. L., "Feasibility Study of Magneto-hydrodynamics Acceleration of Unseeded and Seeded Air Flows," *AIAA Journal*, Vol. 36, No. 4, 1998, pp. 590–597.

[12]Belova, A. V., "Modeling of Electric Discharge Ignition and Combustion of Gaseous Mixtures," M. S. Thesis, The Ohio State Univ., March 2000.

[13]Smith, G. P., Golden, D. M., Frenklach, M., Moriarty, N. W., Eiteneer, B., Goldenberg, M., Bowman, C. T., Hanson, R. K., Song, S., Gardiner, W. C., Jr., Lissianski, V. V., and Qin, Z., http://www.me.berkeley.edu/gri_mech/.

[14]Meyer, R., McEldowney, B., Chintala, N., Palm, P., and Adamovich, I. V., "Experimental Studies of Plasma Assisted Ignition and MHD Supersonic Flow Control," AIAA Paper 2003-0873, Jan. 2003.

[15]McEldowney, B., Meyer, R., Chintala, N., Adamovich, I. V., and Wehe, S., "Ignition of Premixed Hydrocarbon–Air Flows Using a Nonequilibrium RF Discharge," AIAA Paper 2003-3478, June 2003.

[16]Glassman, I., *Combustion*, Academic Press, San Diego, CA, 1996.

[17]Raizer, Y. P., *Gas Discharge Physics*, Springer-Verlag, Berlin, 1991.

[18]Spaulding, D. B., *Some Fundamentals of Combustion*, Gas Turbine Series, Butterworths Scientific, London, 1955.

[19]Suga, M., "Studies on Explosive Reaction of Ethylene Mixed with Oxygen or Air. I. Explosion Limit at Low Pressure," *Journal of Chemical Society of Japan*, Vol. 31, No. 5, 1958, pp. 515–521.

[20]Khitrin, L. N., The Physics of Combustion and Explosion, Moscow Univ. Publishing, 1957.

[21]Pearse, R. W. B., and Gaydon, A. G., *The Identification of Molecular Spectra*, Wiley, New York, 1976.

[22]Bozhenkov, S., Starikovskaia, S., Sechenov, V., Starikovskii, A., and Zhukov, V., "Combustible Mixtures Ignition in a Wide Pressure Range. Nanosecond High-Voltage Discharge Ignition," AIAA Paper 2003-0876, Jan. 2003.

Queries

Q1. Give job/position title./If any of the authors of the current paper are AIAA members, indicate membership category.
Q2. Give job/position title.
Q3. Give job/position title.
Q4. Give job/position title.
Q5. Give job/position title.
Q6. Give job/position title.
Q7. Give job/position title.
Q8. Multiple-part references are treated as multiple entries. Check renumbering.
Q9. Acronyms that are not used again are deleted.
Q10. Figure in the pdf printout was different from figure in the source file; we used the source file. OK?
Q11. Please give dual or metric units for English units in this paper (required for AIAA Journal and JTHT but OPTIONAL for the other journals).
Q12. Spell out cfm.
Q13. Spell out acronym.
Q14. Acronyms that are not used again are deleted./Acronyms that are not used again are deleted.
Q15. Spell out acronym.
Q16. Figure in the pdf printout was different from figure in the source file; we used the source file. OK?
Q17. Figures must be called out in the text in numerical order. Please check renumbering or revise text if you would like original numbering restored.
Q18. Figure in the pdf printout was different from figure in the source file; we used the source file. OK?
Q19. Figure in the pdf printout was different from figure in the source file; we used the source file. OK?
Q20. Figure in the pdf printout was different from figure in the source file; we used the source file. OK?
Q21. Figure in the pdf printout was different from figure in the source file; we used the source file. OK?
Q22. Figure in the pdf printout was different from figure in the source file; we used the source file. OK?
Q23. Figure in the pdf printout was different from figure in the source file; we used the source file. OK?
Q24. Figure in the pdf printout was different from figure in the source file; we used the source file. OK?
Q25. Figure in the pdf printout was different from figure in the source file; we used the source file. OK?
Q26. Figure in the pdf printout was different from figure in the source file; we used the source file. OK?
Q27. References should not be cited for the first time in the Conclusions/Summary section. Please cite earlier or delete.
Q28. References should not be cited for the first time in the Conclusions/Summary section. Please cite earlier or delete.
Q29. Spell out acronym.
Q30. For all refs with single page cited, provide range as appropriate./Give issue number (month is acceptable if there is no issue number).
Q31. Give issue number (month is acceptable if there is no issue number).
Q32. Give issue number (month is acceptable if there is no issue number).
Q33. Give issue number (month is acceptable if there is no issue number).
Q34. Give issue number (month is acceptable if there is no issue number).
Q35. Verify title of article as published or amend.
Q36. Give sponsor/publisher and city of same (not city of conference).
Q37. Verify title of article as published or amend./Multiple-part references are treated as multiple entries. Check renumbering./Give department if applicable.
Q38. Give chapter/article title./Give complete citation date (day-month-year) for URL reference.
Q39. If this was subsequently published in an archival source, give full publication information.
Q40. If this was subsequently published in an archival source, give full publication information.
Q41. Give page range or chapter if applicable.
Q42. Give page range or chapter if applicable.
Q43. Give page range or chapter if applicable.
Q44. Give city of publisher./Give page range or chapter if applicable.
Q45. Give page range or chapter if applicable.
Q46. If this was subsequently published in an archival source, give full publication information.